Nonlinear optical effects in porous silicon: Photoluminescence saturation and optically induced polarization anisotropy

Al. L. Efros and M. Rosen
Nanostructure Optics Section, Naval Research Laboratory, Washington, D.C. 20375

B. Averboukh, D. Kovalev, M. Ben-Chorin, and F. Koch
Technische Universität München, Physik-Department E16, D-85747 Garching, Germany
(Received 21 January 1997)

We present an analysis of strong nonlinear optical effects observed in the photoluminescence of porous Si. Two groups of effects are discussed. The first includes photoluminescence saturation, suppression of the polarization memory, and pump coincident optically induced polarization anisotropy all observed at room temperature. These effects are well described by nonradiative Auger quenching of the photoluminescence in nanocrystals containing more than one electron-hole pair and which are selectively excited by linearly polarized light. The second group is connected with photoluminescence degradation and a persistent optically induced polarization anisotropy at helium temperature. These effects arise from and are very well described by Auger autoionization of crystals selectively excited by polarized light, and subsequent Auger quenching of all radiative recombination in them since they contain long-lived charged carriers. Upon heating the samples to room temperature the electron returns back to the nanocrystal. This restores the initial photoluminescence intensity and washes out the long-lived optically induced polarization anisotropy. The high efficiency of all these effects is provided by the large ratio of the rate of Auger processes to the radiative recombination rate in the nanosize Si crystals. [S0163-1829(97)00731-5]

I. INTRODUCTION

One of the properties possessed by nanocrystal assemblies most important for future applications is their strong nonlinear optical response.[1,2] Nonlinear optical effects in absorption can be observed at relatively low excitation power because a second electron-hole pair in the nanocrystal is excited in the presence of the electric field of the first pair, which affects the transition energy and oscillator strength of the second.[3,4] Stronger nonlinear effects are seen in photoluminescence (PL) because of the high rate of Auger processes in nanocrystals.[5–7] This is because momentum conservation, which leads to a kinematic temperature dependent threshold for Auger processes in the bulk, is absent in nanocrystals,[8] and is also due to the abruptness of the heterointerface between the crystal and the surrounding matrix, which considerably accelerates the rate of Auger processes.[8,9]

Porous silicon films are such assemblies of nanometer size silicon crystals and wires. Their high PL quantum efficiency, discovered recently by Canham,[10] arises from good passivation of the Si nanocrystal surface (see the review of Brus[11]). Experimental[12] and theoretical[13] investigations of porous Si show that silicon nanocrystals still have an indirect band gap: phonon assisted optical transitions are stronger than those for zero phonon lines. As a result porous Si has a small absorption coefficient near the band gap,[14] and a long radiative decay time.[15] The long radiative decay time of the electron-hole (e-h) pairs, milli- to microseconds, makes it very easy to observe the nonlinear behavior in photoluminescence. Highly efficient Auger processes quench all luminescence in nanocrystals which contain more than one e-h pair or which have an unpaired charge. The long-lived charged state leads to PL degradation under light soaking conditions in semiconductor doped glasses, known as the photodarkening effect.[6] These nonlinear processes are much more efficient, however, and can be observed at much lower excitation intensity, in Si nanocrystals where radiative lifetimes are at least three orders of magnitude larger than in doped glasses[16,17] Voltage selective quenching of PL and voltage tunable electroluminescence are also examples of nonlinear optical effects in which nonradiative Auger processes quench the luminescence in Si nanocrystals containing an extra charge.[18,19]

The linear polarization memory effect is yet another effect, observed specifically in the PL of porous silicon films.[20–23] The effect is a result of the nonspherical shape of the nanocrystals which form porous Si films, and which are randomly oriented in the surface plane of the films.[22,24] Linearly polarized light selectively excites those crystals whose largest dimension is parallel to the vector polarization of the exciting light, because the depolarization decreases the component of the electric field along that axis inside the nanocrystal less than it does the other components.[25] Light subsequently emitted by these crystals is also predominantly polarized along the same direction. This results in the strong polarization of the luminescence which depends weakly on the excitation frequency and does not depend on the polarization direction of the exciting light in the surface plane of the porous Si film.

In this paper we study nonlinear optical effects in the photoluminescence of porous silicon: in particular, saturation of the PL intensity at room temperature and PL photodegradation at low temperature. The saturation of room temperature photoluminescence at high excitation intensity is a result of nonradiative Auger recombination in nanocrystals containing two e-h pairs. The PL photodegradation is a result of

Auger autoionization of the nanocrystals and the subsequent Auger quenching of all further radiative recombination in the charged nanocrystals. Both these effects are seen especially clearly in PL polarization pump-probe experiments in which we selectively saturate nanocrystals whose largest dimension is parallel to the vector polarization of the pump beam or in which we selectively degrade nanocrystals whose largest dimension is along the vector polarization of the degrading light. These polarization studies are a kind of differential technique, separating out the contribution of the strongly saturated (degraded) and the weakly saturated (degraded) nanocrystals. At room temperature the selectively saturated nanocrystals show the strong in-surface-plane polarization anisotropy of the probe beam PL which occurs simultaneously with the pump beam. At low temperature the selective photodegradation produces a long-lived polarization anisotropy. These nonlinear effects are well described within the framework of a model which considers porous silicon as an aggregate of randomly oriented dielectric ellipsoids which emit light only if they contain a single electron-hole pair.

In Sec. II we describe the polarization properties of an aggregate of randomly oriented dielectric ellipsoids. In Sec. III we discuss the specifics of the experimental setup and the samples studied. In Sec. IV we consider the saturation of the photoluminescence and the decrease of the degree of polarization in porous Si at room temperature under high excitation conditions. Section V deals with the photoluminescence degradation and the long-lived optically induced polarization anisotropy seen at low temperature. Conclusions are drawn in Sec. VI.

II. THEORY

Let us consider the polarization properties of the porous Si PL observed in Refs. 20–23. It was shown that the polarization is a result of the nonsphericity of the nanocrystals in the porous Si.[22,24] The effect arises from the large difference between the dielectric constant of the anisotropic semiconductor crystals and the surrounding medium. Similar optical effects due to dielectric differences were first demonstrated for open semiconductor quantum well wires.[26]

We shall assume that porous Si is an aggregate of both elongated and flattened ellipsoidal dielectric Si crystals preferentially oriented in the [100] growth direction of the *p*-Si film, and embedded in an effective dielectric medium.[16] In this model the electric field $\mathbf{E}^i$ inside a dielectric ellipsoid is related to the external field $\mathbf{E}^o$ of the exciting or emitted (and detected) light by

$$E^i_{x,y,z}=E^o_{x,y,z}/[1+n^{(x),(y),(z)}\delta(\omega)], \tag{1}$$

where $\delta(\omega)=[\varepsilon_i(\omega)/\varepsilon_o(\omega)]-1$, $\varepsilon_i(\omega)$ and $\varepsilon_o(\omega)$ are the dielectric constants of Si and the effective medium, respectively (both constants depend on the frequency ω of the light). The depolarization factors, $n^{(x),(y),(z)}$, depend on the semiaxis dimensions of the ellipsoid (a, b, and c), for ellipsoids of revolution:[25]

$$n^{(z)}=\begin{cases}\dfrac{1-e^2}{2e^3}\left(\ln\dfrac{1+e}{1-e}-2e\right)\leqslant\dfrac{1}{3} & \text{if} \quad a=b<c\\[2ex] \dfrac{1+e^2}{e^3}(e-\arctan e)\geqslant\dfrac{1}{3} & \text{if} \quad c<a=b,\end{cases} \tag{2}$$

$$n^{(x)}=n^{(y)}=[1-n^{(z)}]/2, \quad e=\sqrt{\left|1-\frac{a^2}{c^2}\right|}. \tag{3}$$

One can see from Eqs. (1), (2) that, because the depolarization factors for longer axes are less than those for the shorter axes, the decrease in the component of the electric field along a long axis is less than that along a short axis [in the limit of very elongated nanocrystals ($c\gg a$), $n^{(z)}=0$, and the z components of the external and internal electric field are equal].

The probability of nanocrystal excitation is proportional to the square of the electric field, $(\mathbf{E}^i)^2$, inside the nanocrystal. Taking into account the depolarization factors and assuming isotropy of the interband matrix elements, we obtain the angular dependence of the probability of optical excitation of an ellipsoidal dielectric nanocrystal on the angle between the vector polarization of the exciting light, $\mathbf{e}_{\rm ex}$, and a unit vector, $\hat{\mathbf{c}}$, directed along the major ellipsoid axis:

$$P(\omega_{\rm ex})=1+\kappa(\omega_{\rm ex})(\hat{\mathbf{c}}\cdot\mathbf{e}_{\rm ex})^2. \tag{4}$$

The function κ is determined by the shape of the ellipsoid and by the frequency of the exciting light, $\omega_{\rm ex}$:

$$\kappa(\omega)=\frac{\delta(\omega)(1-3n^{(z)})[4+\delta(\omega)(1+n^{(z)})]}{4[1+\delta(\omega)n^{(z)}]^2}. \tag{5}$$

The probability of spontaneous photon emission is also proportional to the square of the electric field, $(\mathbf{E}^i)^2$, of a single photon inside the nanocrystal. The magnitude of this field outside the nanocrystal is determined by the photon energy. The electric field of the emitted photon inside the crystal has to satisfy Eqs. (1) and (2), and therefore is largest for photons whose polarization vector is along the nanocrystal largest dimension. As a result the nanocrystal emits light which is predominantly polarized along its largest dimension. The probability of photon emission has a similar dependence to that for excitation on the angle between the vector polarization of the detected light, $\mathbf{e}_{\rm de}$, and $\hat{\mathbf{c}}$: $P(\omega_{\rm de})=1+\kappa(\omega_{\rm de})(\hat{\mathbf{c}}\cdot\mathbf{e}_{\rm de})^2$, where κ is now calculated at the frequency of the detected light $\omega_{\rm de}$. The resulting intensity of the PL of a single ellipsoidal crystal has the angular dependence, $I_{\rm PL}\sim P(\omega_{\rm ex})P(\omega_{\rm de})$. This expression, averaged over the distribution of ellipsoid shapes and orientations, describes the linear polarization effects in porous Si.[22,24]

Nonlinear optical effects take place in any aggregate of nanocrystals when one excites more than one *e-h* pair in a single nanocrystal or causes an unpaired free electron or hole to occur there. In porous Si, however, these nonlinear effects are observed in photoluminescence at much lower excitation intensities than in direct semiconductors; this is a consequence of the very long radiative lifetimes $\tau_r\sim 10$–$100\ \mu$s occurring in Si crystallites. This makes it much easier to excite a second *e-h* pair in a nanocrystal before the first one has recombined. Furthermore, the slow radiative recombination cannot compete with the fast nonradiative Auger processes whose typical times are on the order of a nanosecond.[9,19] An excited electron-hole pair recombines radiatively, and emits light, only if the crystal did not already contain an *e-h* pair or free carriers before excitation. As a result, the total intensity of the PL can be written:

$$I_{\mathrm{PL}} \sim \langle N_0(\hat{\mathbf{c}}) P(\omega_{\mathrm{ex}}) P(\omega_{\mathrm{de}}) \rangle, \tag{6}$$

where $N_0(\hat{\mathbf{c}})$ is the probability that the crystal contains no free electrons and/or holes and $\langle\ \rangle$ denotes averaging over the distributions of crystal shapes and orientations. This expression does not take into account spatial diffusion of the excited *e-h* pairs to other crystallites in the aggregate, and also assumes that there are no nonradiative channels associated with internal or surface defects. Using the polarized light of an optical pump beam, we can selectively excite crystals whose largest dimension is parallel to the polarization of the pump [see Eq. (4)] and in this way prepare a temporary or permanent anisotropic in-surface plane distribution of unexcited crystals. This distribution is reflected in the angular dependence of the PL intensity, I_{PL}, and leads to polarization anisotropy effects. In Sec. IV we discuss the effect of a polarized pump beam which creates a temporary anisotropic distribution, $N_0(\hat{\mathbf{c}})$, coexisting simultaneously with the pump at room temperature. This distribution is reflected both in the polarization memory effect and in the polarization of the probe induced PL. In Sec. V we discuss the permanent degradation of the photoluminescence by polarized light at low temperature, where a permanent anisotropic distribution, $N_0(\hat{\mathbf{c}})$, results from nanocrystal ionization.

III. EXPERIMENTAL NOTES

Microporous silicon layers are prepared from *p*-type (100), boron doped substrates with a typical resistivity of 5 Ω cm. The electrochemical etching is done in a teflon cell containing ethanoic hydrofluoric solution, using a Pt wire as a cathode and an etch current density of 30 mA/cm^2. The etching solution is a 1:1 by volume mixture of hydrofluoric acid (49% wt. in water) and ethanol. The layer thicknesses are chosen from 1 to 10 μm to provide uniform optical excitation within the layer. For some experiments free standing layers are used. They are detached from the substrate by electropolishing. All the samples are fabricated in the dark and are aged for several months after preparation in order to increase their PL efficiency.

The experiments are done using a pump-probe technique. For the pump, a high intensity (up to 600 W/cm^2) cw Ar^+ or dye laser beam is used. The pump beam is linearly polarized in the plane of the sample. The detected emission is excited using a weak polarized probe beam. The light of both the pump and the probe beams are deflected using small mirrors and are incident onto the sample normal to the surface plane. Coincidence of the pump laser spot with the smaller diameter probe laser spot is controlled by an optical microscope. The emitted light is collected by the lenses of a condenser and focused onto the entrance slit of a monochromator. The polarization of the detected light is determined by a polarizer placed between the lenses of the condenser, where the beam is parallel. A depolarizer is mounted at the entrance slit of the monochromator, in order to avoid problems with the polarization properties of the grating. All PL spectra are normalized for the spectral response of the optical detection system.

The source of the probe beam is a second Ar^+ laser operating at 4880 Å or a He-Cd laser (4420 Å). Its polarization relative to that of the pump beam is determined by a system of a depolarizer and a linear polarizer. Rotating the polarizer rotates the polarization vector of the exciting light in the sample surface plane; its angle with respect to that of the pump beam can be tuned. The probe beam is chopped (the pump is operating in cw mode) and the usual lock-in technique is used to measure coherently the PL response to the probe beam. For PL lifetime measurements a pulsed N_2 laser with a 300 ps pulse length and a 10 Hz repetition rate is used. The excitation intensity at $\hbar\omega = 3.67$ eV is 100 W/cm^2. The resolution time of the detection system for the lifetime measurements is better than 5 ns. The PL lifetimes are obtained from a single exponential fit to the multiexponential temporal PL kinetics. As a pump source, a variable intensity Ar^+ laser (4880 Å) is used. At the large cw optical excitation intensities, special care is taken to avoid the influence of the room temperature PL degradation on the results of measurements which could arise, e.g., from heating. All measurements at high optical intensities are made after an initial degradation. The procedures described above are for the room temperature measurements.

The low temperature ($T = 5$ K) PL fatigue effects were studied after an initial illumination of the samples with the 4880 Å linearly polarized line of a cw Ar^+ laser at an intensity of 20 W/cm^2 for 20 min. Afterwards, the PL excited with the 4420 Å linearly polarized line of a He-Cd laser and its degree of polarization are measured for different polarization directions relative to that of the degraded light. We found no difference between measurements done within about ten hours after the initial degradation.

IV. ROOM TEMPERATURE NONLINEAR PL EFFECTS

A. PL saturation and polarization memory effect

The photoluminescence of porous Si shows very strong nonlinear effects at relatively weak excitation intensities. Typical PL and the degree of polarization spectra obtained for our samples at low excitation intensity are shown in the inset of Fig. 1. The PL is linearly polarized throughout the entire spectral range; the degree of linear polarization varies from 0.2 at the high energy edge of the spectrum to 0.05 at the red one, in agreement with previous reports.[21–23] Figure 1 shows the dependence of the PL intensity, its decay lifetime, and the degree of linear polarization on the cw excitation intensity for several detection energies. The PL intensity increases linearly with the excitation intensity, I_{ex}, up to ~ 2 W/cm^2, above which saturation effects are observed. The deviation from the linear behavior is stronger, and starts at lower excitation intensities for lower detection energies [Fig. 1(a)]. This results in a blueshift of the whole PL spectrum with excitation intensity.[17] Lifetimes, measured as a function of the pump beam intensity, do not change at low excitation intensities but decrease in the PL saturation regime [see Fig. 1(b)]. One sees a strong correlation between the PL saturation and the radiative lifetime of the nanocrystals contributing to the PL. The PL saturation threshold is lower for nanocrystals having longer radiative lifetimes [compare Figs. 1(a) and 1(b)]. The decrease of the radiative lifetimes at high excitation intensity shown in Fig. 1(b) is also a reflection of the PL saturation in crystals with long radiative lifetimes. The lifetimes shown in Fig. 1(b) are ob-

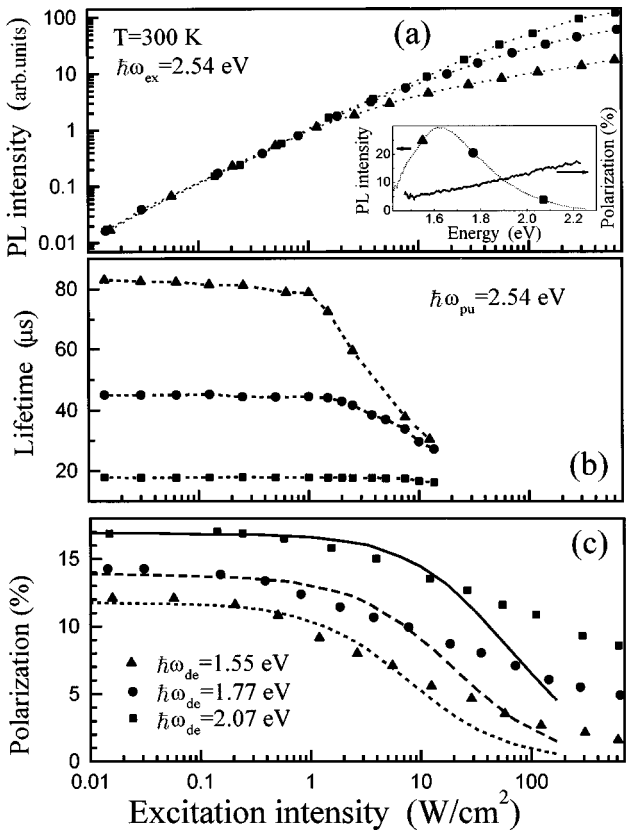

FIG. 1. (a) PL intensity versus cw excitation intensity for three different detection energies: 2.07 eV (squares), 1.77 eV (circles), and 1.55 eV (triangles). The excitation energy is 2.54 eV. (b) PL lifetimes versus cw pump intensity for the same detection energies. The PL is excited by a 300 ps pulsed N_2 laser at an energy of 3.67 eV. (c) The degree of the PL linear polarization versus an excitation intensity for the same detection energies. The curves are theoretical fits. Inset: PL spectrum (dotted line) and the degree of PL linear polarization (solid line) at an excitation intensity of 1 W/cm^2.

tained from the monoexponential fit to the multiexponential decay curves, i.e., the crystals luminescing at the same frequency have a distribution of radiative lifetimes. The saturation of the PL at high excitation intensities of those crystals that have long radiative lifetimes leads to an effective decrease in the lifetimes obtained from this monoexponential fit to the data.

The effect of the PL saturation is clearly seen in the polarization memory effect measurements [see Fig. 1(c)]. The degree of linear polarization is even more sensitive than the PL to the excitation intensity and to the detection frequencies. It is independent of I_{ex} at low excitation intensity and decreases after some critical intensity, dependent on the detection frequency, in the range 0.2–0.4 W/cm^2. This behavior arises from the selective saturation of nanocrystals whose largest dimension is parallel to the polarization of the exciting light and the consequent decrease of the PL quantum efficiency of these crystals. To describe this behavior we consider nanocrystal state filling rate equations for cw polarized excitation:

$$\dot{N}_0=\frac{N_1}{\tau_r}-N_0W_e[1+\kappa(\omega_{ex})(\hat{\mathbf{c}}\cdot\mathbf{e}_{ex})^2],$$

$$\dot{N}_1=\frac{N_2}{\tau_A}+(N_0-N_1)W_e[1+\kappa(\omega_{ex})(\hat{\mathbf{c}}\cdot\mathbf{e}_{ex})^2]-\frac{N_1}{\tau_r},$$

$$\dot{N}_2=N_1W_e[1+\kappa(\omega_{ex})(\hat{\mathbf{c}}\cdot\mathbf{e}_{ex})^2]-\frac{N_2}{\tau_A}, \tag{7}$$

where N_0, N_1, and N_2 are the concentrations of nanocrystals with the major axis along $\hat{\mathbf{c}}$ and which contain 0, 1, and 2 e-h pairs, respectively ($N_0+N_1+N_2=N$), $W_e=I_{ex}\alpha(\omega_{ex},a)$ is the average probability for exciting a nanocrystal, where $\alpha(\omega_{ex},a)\hbar\omega_{ex}$ is the effective absorption cross section which depends both on the excitation frequency, ω_{ex}, and the average crystal size a (far from the band edge it is the same for both the first and the second excited e-h pair). τ_r is the radiative lifetime of a single e-h pair and $1/\tau_A$ is the rate of nonradiative Auger recombination in nanocrystals with two e-h pairs. We consider only relatively low excitation intensities, I_{ex}, where $I_{ex}\alpha\tau_A\ll 1$ and the excitation probability of more than two e-h pairs is negligibly small. For these conditions, Eq. (7) give the steady state concentration of unexcited nanocrystals $N_0(\hat{\mathbf{c}},\mathbf{e}_{ex})$:

$$N_0(\hat{\mathbf{c}},\mathbf{e}_{ex})=\frac{N}{1+\tau_rI_{ex}\alpha(\omega_{ex},a)[1+\kappa(\omega_{ex})(\hat{\mathbf{c}}\cdot\mathbf{e}_{ex})^2]}. \tag{8}$$

The intensity of the PL polarized parallel (perpendicular), $I_\parallel(I_\perp)$, to the vector polarization of the exciting light is obtained substituting this function into Eq. (6), from which we obtain a full description of the degree of polarization $\rho=(I_\parallel-I_\perp)/(I_\parallel+I_\perp)$.

Although the polarization vectors of the exciting, $\mathbf{e}_{ex}$, and detected, $\mathbf{e}_{de}$, light are in the surface plane of the porous Si film in our experiments, the averaging over the distribution of nanocrystal axes $\hat{\mathbf{c}}$ in Eq. (6) has a three dimensional character. Henceforth, we will use the simplifying assumption that all crystals contributing to the PL at a particular frequency have the same shape (characterized by $n^{(z)}$), size, radiative lifetime, and have their $\hat{\mathbf{c}}$ axes aligned at an angle γ relative to the [100] p-Si growth direction, $\cos\gamma=(\hat{\mathbf{c}}\cdot[100])$, and that their axes of revolution are randomly distributed about this direction. With this we obtain the dependence of the PL intensity on the azimuthal angles, φ_e and φ_d, of the vector polarizations of the exciting and detected light, respectively:

$$I_{PL}\propto\frac{2}{\tau_rW_e\kappa_e}\{(2+\kappa_e)(2+\kappa_d)I_0(b_e)+(2+\kappa_d)\kappa_eI_1(b_e)+\cos2(\varphi_e-\varphi_d)[(2+\kappa_e)\kappa_dI_1(b_e)+\kappa_e\kappa_dI_2(b_e)]\}, \tag{9}$$

where $\kappa_{e,d}=\kappa(\omega_{ex,de})\sin^2\gamma$, $I_0(x)=1/\sqrt{x^2-1}$, $I_1(x)=1-xI_0(x)$, $I_2(x)=-xI_1(x)$, and the parameter of nonlinearity $b_e=[2+\tau_rW_e(2+\kappa_e)]/\tau_r\kappa_eW_e$ depends on the excitation frequency and the intensity $[W_e=I_{ex}\alpha(\omega_{ex},a)]$. Equation

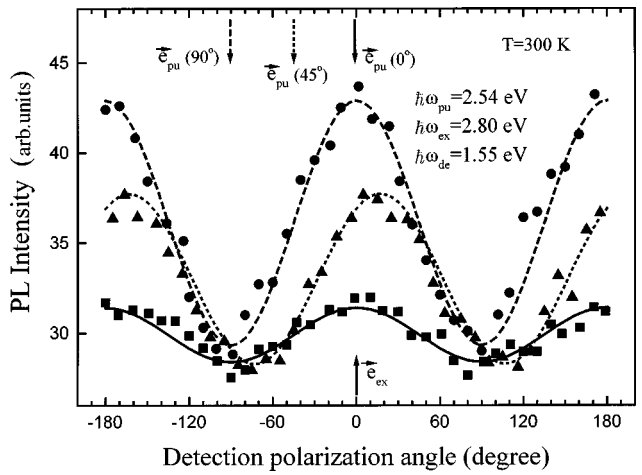

FIG. 2. Dependence of the porous silicon PL intensity on the angle between the polarizations of exciting and detected light for three polarization directions of the pump beam. Pump and probe beam polarizations are indicated by the arrows. The curves are theoretical fits.

(9) coincides with Eq. (5) of Ref. 22 at low excitation intensity and gives $\rho=0$ at high excitation intensity, when $\tau_r W_e \gg 1$.

Using Eq. (9) we describe the dependence of the degree of polarization on the intensity of the exciting light, shown in Fig. 1(c). The best description is obtained with values of $\alpha(\hbar\omega_{ex}=2.54\ \text{eV},a)=3.9\times10^{-17}$, 2.3×10^{-17}, and 1.4×10^{-17} cm^2/eV; $n^{(z)}=0.08$, 0.05, and 0.01; and $\sin\gamma=0.57$, 0.50, and 0.45 for the detection frequencies $\hbar\omega_{de}=1.55$, 1.77, and 2.07 eV, respectively. We also used the average experimental values of $\tau_r=82$, 45, and 19 μs. The decrease in α with detection energy is well correlated with the decrease in the size of those crystals contributing to the PL at higher luminescence energy. The disagreement at high excitation intensity arises from the wide distribution of radiative lifetimes of the crystals emitting at the same energy. One can see, for example, in the luminescence decay curves at detection energy 1.55 eV, a distribution of τ_r from 105 to 22 μs. This distribution washes out the rapid transition to zero polarization predicted theoretically, because saturation of crystals with shorter radiative lifetimes occurs at higher excitation intensities.

B. Optically induced photoluminescence polarization anisotropy

We also examine optically induced saturation of the PL using a pump-probe technique. Anisotropic distributions of saturated nanocrystals are prepared by a high intensity (up to 600 W/cm^2) polarized beam, which selectively saturates crystallites whose largest dimension is parallel to the vector polarization of the pumping light. The effect of this anisotropic distribution is monitored by studying the PL intensity caused by a weak linearly polarized probe beam. The PL intensity as a function of its polarization angle is shown in Fig. 2 for three different angles between the vector polarization of the pump and probe beams (0°, 45°, and 90°). The polarization direction of the detected light is defined with respect to the direction of the polarization of the probe beam. The 180° periodicity of the PL intensity in all cases is very apparent. The intensity of the PL decreases considerably when the vector polarization of the probe light approaches the direction of the pump beam polarization, because the probe beam is then probing those nanocrystals that have been selectively saturated by the pump beam. The pump beam polarization introduces a direction, an anisotropy, in the sample surface plane. The resultant anisotropic distribution of pumped crystals leads to a phase shift in the dependence of the intensity of the probe beam PL on the angle between the polarizations of the exciting and detected light when the polarization vector of the probe is not parallel or perpendicular to the pump beam. The shift is a maximum when the angle between the vector polarization of the pump and probe beams is 45° (see triangles in Fig. 2). The magnitude of the shift increases with the intensity of the pump.

To describe the PL intensities shown in Fig. 2 we use Eq. (6) with $N_0(\hat{\mathbf{c}},\mathbf{e}_{pu})$ being given by Eq. (8) calculated for the intensity and polarization of the pump beam. Using the approximation described above, we find the dependence of the probe beam PL intensity on the azimuthal angles of the vector polarization of exciting, φ_e, and detected, φ_d, light:

$$
\begin{aligned}
I_{\mathrm{PL}} \propto \frac{2}{\tau_r W_p \kappa_p}\{&[(2+\kappa_e)(2+\kappa_d) \\
&+\kappa_e\kappa_d \sin 2\varphi_e \sin 2\varphi_d] I_0(b_p) \\
&+[(2+\kappa_d)\kappa_e \cos 2\varphi_e + (2+\kappa_e)\kappa_d \cos 2\varphi_d] I_1(b_p) \\
&+\cos 2(\varphi_e+\varphi_d) I_2(b_p)\}, \qquad (10)
\end{aligned}
$$

where φ_e and φ_d are calculated relative to the vector polarization of the pump light, $\kappa_p=\kappa(\omega_{pu})\sin^2\gamma$, and the parameter of nonlinearity $b_p=[2+\tau_r W_p(2+\kappa_p)]/\tau_r\kappa_p W_p$ depends on the excitation frequency, ω_{pu}, and intensity, I_{pu}, of the pumping light $[W_p=I_{pu}\alpha(\omega_{pu},a)]$. Using this expression and the same parameters which gave the best fit to the PL polarization in Fig. 1(c), we have reproduced the experimental dependences in Fig. 2.

The anisotropy of the selectively saturated distribution of nanocrystals is better seen in the dependence of ρ on the angle between the polarization of the probe and the pump beams. Figure 3 shows this dependence for two values of pump intensity. ρ is isotropic in the surface plane in the absence of the pump beam. This is a consequence of the macroscopic isotropy of the porous silicon PL (Refs. 21 and 22) in the plane perpendicular to the [100] p-Si growth direction. The polarized pump beam clearly induces an anisotropy which is related to the direction of the pump beam polarization (shown by the arrow) and increases with the pump intensity. One sees that, for parallel pump and probe polarizations, ρ is $\sim$4% at high excitation intensity and becomes about 8% in the absence of the pump beam. Using Eq. (10) we determine the angular dependence of ρ for zero and high pump beam intensities. The fit shown on Fig. 3 used the same parameters as in Fig. 1(c). We note here that the probe beam intensity (2 W/cm^2) was chosen a bit beyond the range where ρ is constant [Fig. 1(c)] in order to maintain a reasonable signal-to-noise ratio.

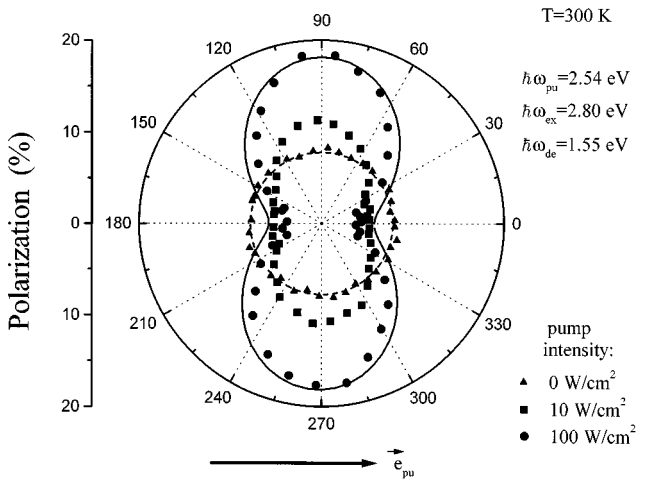

FIG. 3. Polar plot of the room temperature PL polarization as a function of the polarization direction of the probe beam for three pump beam intensities. The direction of the pump beam polarization is indicated by the arrow. The curves are theoretical fits.

C. PL quenching at resonant excitation

In principle, optically induced polarization anisotropy could also arise from the modification of the absorption coefficient of crystallites containing an *e-h* pair (or an unpaired free charge) because the electric field of the charges could affect further absorption in these nanocrystals. Furthermore in nanocrystals with well separated quantized levels, the Pauli principle acting in the lowest lying states leads to bleaching of the band-edge absorption. However this is not the case in porous Si—our absorption measurements on free standing *p*-Si layers for the same experimental configuration do not show any influence of the pump beam on the absorbance of the probe. This is probably connected with the high density of the band-edge exciton states in Si nanocrystals. A multiband effective mass estimate shows that there are at least 48 band-edge exciton states in spherical Si nanocrystals.

To prove that the polarization anisotropy effect is connected with photoluminescence intensity saturation, we examined the spectral dependence of the PL intensity and of ρ for the case of resonant pumping into the emission band (see Fig. 4). The PL spectrum of porous silicon is inhomogeneously broadened by the wide distributions of nanocrystal sizes and shapes which determine the positions of the electron and hole lowest quantum size levels. The PL of each nanocrystal is determined by transitions between these levels. Thus, at resonant excitation, we selectively excite those crystals whose emission band edge is below the pumping frequency. Figure 4(a) shows, for a pumping frequency $\hbar\omega_{pu}=1.96$ eV and an excitation energy $\hbar\omega_{ex}=2.54$ eV, that the PL spectrum below the energy of the pump beam is partially quenched, but the luminescence with an energy higher than the pump beam is not affected. The spectral behavior of ρ for two probe beam polarization directions relative to that of the pump beam (parallel and perpendicular) is shown in Fig. 4(b). The variation in ρ correlates very well with the measurements made for nonresonant pumping (see Figs. 2 and 3); however, there they were seen only for the

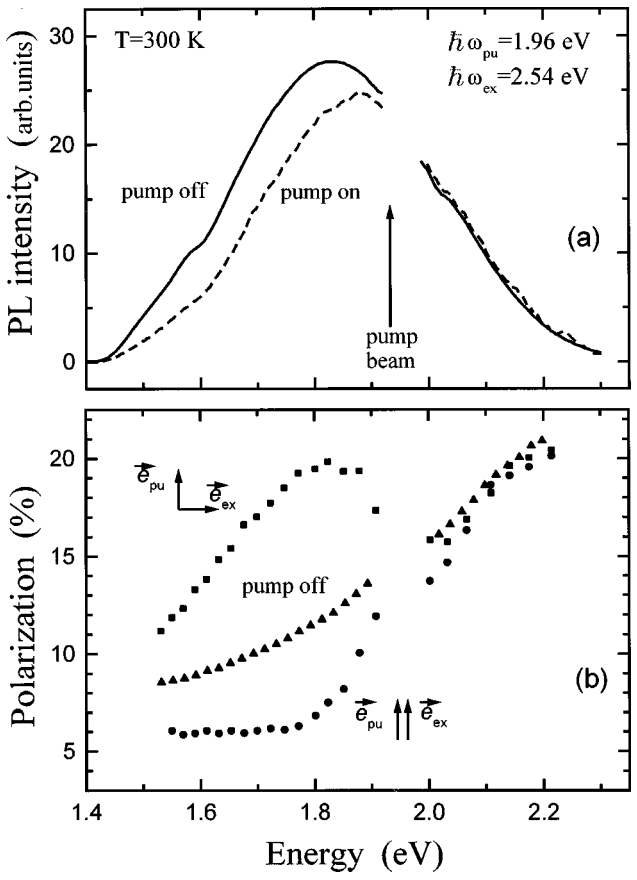

FIG. 4. The effect of the resonant pump beam excitation on the PL (a) and the PL polarization spectra (b). The effect on the PL polarization is shown both for the case when the probe beam polarization is parallel to and perpendicular to that of the pump beam. The break in the curves occurs in the spectral cutoff region of the notch filter placed in front of the monochromator in order to suppress the pump beam radiation.

states below the pump energy. The spectral dependence of the deviation from ρ measured in the absence of a pump beam correlates well with the suppression of the PL intensity. These data rule out the nonlinear absorption model of polarization anisotropy in explaining our experiments.

V. LOW TEMPERATURE PL DEGRADATION

The PL from porous Si exhibits a low temperature fatigue phenomenon. The PL can be efficiently quenched by intense cw illumination at liquid helium temperature and does not recover for hours. Figure 5(a) shows the low temperature porous Si PL spectra before and after degradation of the sample by strong cw polarized light for a period on the order of 20 min. The PL intensity decreases drastically after degradation, but heating the samples back up to room temperature restores the initial intensity. This fatigue phenomenon is connected with the Auger autoionization of the nanocrystals, when two electron-hole pairs are optically excited, with subsequent Auger quenching of all further radiative recombination in the charged nanocrystals.[16,27] The electron ejected from the Si crystal is localized on a trap in the matrix. Heat-

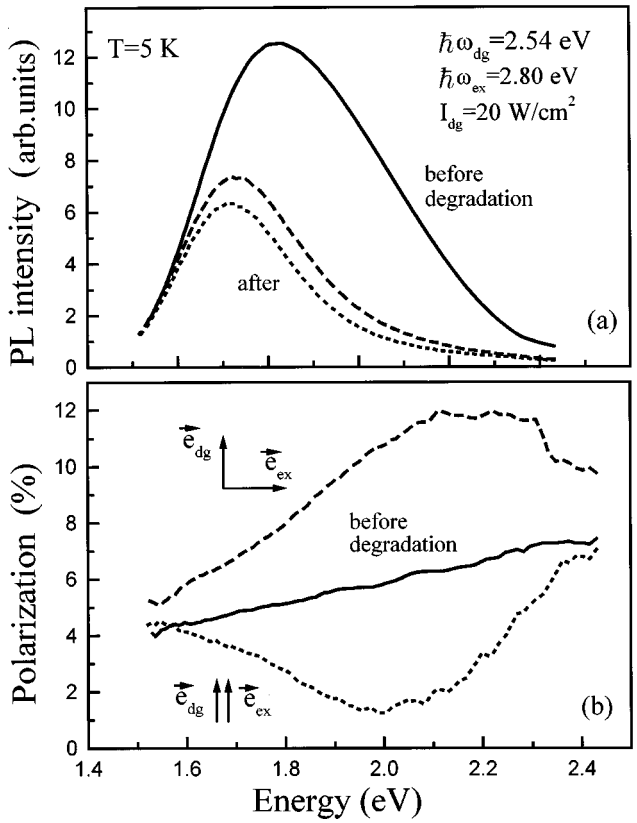

FIG. 5. The effect of optical degradation by a 20 min illumination by a 20 W/cm^2 4880Å line of a polarized cw Ar^+ laser pump beam on the PL (a) and the PL polarization (b) spectra. The effect on the PL and on the PL polarization spectrum is shown for the probe beam polarization both parallel (dotted line) and perpendicular (dashed line) to that of the degrading pump beam.

ing of the sample returns the electron back to the crystal and restores its initial optical properties.

One can notice in Fig. 5(a), that degradation changes the porous Si PL spectrum mainly at the high energy part of the emission spectrum, while the red tail of the spectrum is almost unaffected. The changes in PL are most pronounced in the region 1.8–2.2 eV, which is directly related to the efficiency of Auger autoionization. The autoionization rate was shown to strongly depend on the nanocrystal radius, $\overline{a}$.[9] It varies as $(\overline{a})^{-\nu}$, where ν ranges from 5 to 7, depending on the value of the band offset. Auger autoionization can take place only if the band offset for one of the carriers is smaller than the effective energy gap of the nanocrystal. Both these effects lead to more efficient Auger autoionization in small nanocrystals. The effective energy gap of these nanocrystals is larger due to the quantum size effect and, when they emit light they do so at a relatively higher frequency. This is the reason for the redshift of the PL after optical degradation of the porous Si films.

The effect of the PL degradation in porous Si is clearly seen if the probe light is polarized. The intensity of the PL excited by light whose vector polarization is parallel to that of the degrading light is lower than in the perpendicular geometry [see Fig. 5(a)]. This brings about the long-lived optically induced polarization anisotropy.[16] Figure 5(b) shows the spectral dependence of the degree of linear polarization both before and after degradation of the sample by polarized light. The initial values of ρ vary from 0.04 to 0.08, and do not depend on the direction of the vector polarization of the exciting probe light. After degradation by linearly polarized light, the degree of polarization changes drastically. When the directions of the vector polarization of the degrading and the probe beams are parallel, the degree of linear polarization is lower over the whole spectral range of the PL; for the perpendicular polarization excitation geometry, ρ is higher. This effect is a consequence again of Auger autoionization of selectively excited crystals and disappears completely after heating the samples up to room temperature. This selective degradation process involves a competition between crystal Auger ionization and crystal neutralization due to thermally induced return of the electron back to the crystal. It is described by the nanocrystal state filling rate equations for cw excitation at a low temperature:

$$\dot{N}_0=\frac{N_1}{\tau_r}-N_0W_d[1+\kappa(\omega_{dg})(\hat{\mathbf{c}}\cdot\mathbf{e}_{dg})^2],$$

$$\dot{N}_1=\frac{N_+}{\tau_T}+(N_0-N_1)W_d[1+\kappa(\omega_{dg})(\hat{\mathbf{c}}\cdot\mathbf{e}_{dg})^2]-\frac{N_1}{\tau_r},$$

$$\dot{N}_2=N_1W_d[1+\kappa(\omega_{dg})(\hat{\mathbf{c}}\cdot\mathbf{e}_{dg})^2]-\frac{N_2}{\tau_{AA}}, \qquad (11)$$

$$\dot{N}_+=\frac{N_2}{\tau_{AA}}-\frac{N_+}{\tau_T},$$

where N_+ is the concentration of ionized nanocrystals with main axis along $\hat{\mathbf{c}}$, the total crystal concentration $N=N_0+N_1+N_2+N_+$ at low temperature, $W_d=I_{dg}\alpha(\omega_{dg},a)$ is the average probability for exciting a nanocrystal at the excitation frequency, ω_{dg}, I_{dg} is the intensity of the degrading light, $1/\tau_{AA}$ is the rate of Auger autoionization of nanocrystals with two e-h pairs (which we assume does not depend on its shape), and $\tau_T=\tau_{ph}\exp(-\Delta E/kT)$ is the temperature dependent electron return time from the trap in the matrix back to the nanocrystal, ΔE is the depth of the trap, T is the temperature, and τ_{ph} is a typical phonon scattering time. We consider only relatively low excitation intensities where $I_{dg}\alpha\tau_{AA}\ll 1$ and the excitation probability of more than two e-h pairs is negligibly small. For these conditions, Eq. (11) give for the angular distribution of neutral crystals after sample degradation, $N_0(\hat{\mathbf{c}},\mathbf{e}_{dg})$:

$$N_0(\hat{\mathbf{c}},\mathbf{e}_{dg})=\frac{1+S(\hat{\mathbf{c}},\mathbf{e}_{dg})+(\tau_{AA}/\tau_r)S^2(\hat{\mathbf{c}},\mathbf{e}_{dg})}{1+S(\hat{\mathbf{c}},\mathbf{e}_{dg})+[(\tau_T+\tau_{AA})/\tau_r]S^2(\hat{\mathbf{c}},\mathbf{e}_{dg})}, \qquad (12)$$

where $S(\hat{\mathbf{c}},\mathbf{e}_{dg})=\tau_rW_d[1+\kappa(\omega_{dg})(\hat{\mathbf{c}}\cdot\mathbf{e}_{dg})^2]$. Substituting Eq. (12) into Eq. (6), one obtains the angular dependence of the PL intensity of polarized light from the degraded samples:

$$I_{\mathrm{PL}} \propto \frac{\tau_{AA}}{\tau_{AA}+\tau_T}\left[(2+\kappa_e)(2+\kappa_d)+\frac{\kappa_e\kappa_d}{2}\cos 2(\varphi_e-\varphi_d)\right]$$

$$+\left[(2+\kappa_e)(2+\kappa_d)+\frac{\kappa_e\kappa_d}{2}\cos 2(\varphi_e-\varphi_d)\right]$$

$$\times[c_d J_0+d_d J_1]+[(2+\kappa_d)\kappa_e\cos 2\varphi_e$$

$$+(2+\kappa_e)\kappa_d\cos 2\varphi_d]$$

$$\times[c_d J_1+d_d J_2]+\frac{\kappa_e\kappa_d}{2}\cos 2(\varphi_e+\varphi_d)$$

$$\times[c_d(2J_2-J_0)+d_d(J_3-J_1)], \qquad (13)$$

where φ_e and φ_d are measured relative to the vector polarization of the degrading light, analytical expressions for the integrals $J_n(I_{\mathrm{dg}})$, which arise from averaging over the azimuthal distribution of the $\hat{\mathbf{c}}$ axes of the p-Si crystallites, can be found in the Appendix, and the parameters

$$c_d=\left(\frac{\tau_T}{\tau_{AA}+\tau_T}\right)^2\frac{1+S_r(2+\kappa_{dg})}{S_r S_T(\kappa_{dg})^2},$$

$$d_d=\left(\frac{\tau_T}{\tau_{AA}+\tau_T}\right)^2\frac{1}{\kappa_{dg}S_T}, \qquad (14)$$

where $\kappa_{dg}=\kappa(\omega_{\mathrm{dg}})\sin^2\gamma$ depends on the frequency of the degrading light, ω_{dg}, and $S_{r,T}=\tau_{r,T}W_d/2$.

We can use Eq. (13) for describing the dependence of ρ on the direction of the exciting light polarization relative to that of the degrading light at low excitation intensity, when the probe light should not cause saturation of uncharged nanocrystals. From Eq. (8) one can see that the saturation condition is $\tau_r I_{\mathrm{ex}}\alpha\sim 1$, which goes as τ_r. This is two orders of magnitude larger at liquid helium temperature than at room temperature, reaching 10^{-4}–10^{-2} s. As a result, even a probe beam intensity of 0.5 W/cm^2 leads to partial saturation of the crystal and a decrease in ρ. The measured polarization for undegraded samples at liquid helium temperature is only 8% (see Fig. 6), almost half that at room temperature, which shows that saturation caused by the probe beam itself needs to be taken into account.

Figure 6 shows the angular dependence of the degree of linear polarization before (triangles) and after initial illumination of the sample for 20 min. with the 4880 Å linearly polarized emission line of a cw Ar^+ laser with an intensity 100 W/cm^2 (circles). The PL was excited with the 4420 Å linearly polarized emission line of a He-Cd laser with an intensity 0.5 W/cm^2. After degradation the PL shows a strong anisotropy caused by Auger autoionization of the selectively excited crystals. To describe this angular dependence the saturation caused by the probe beam has to be taken into account. For this case, instead of Eq. (6) we have

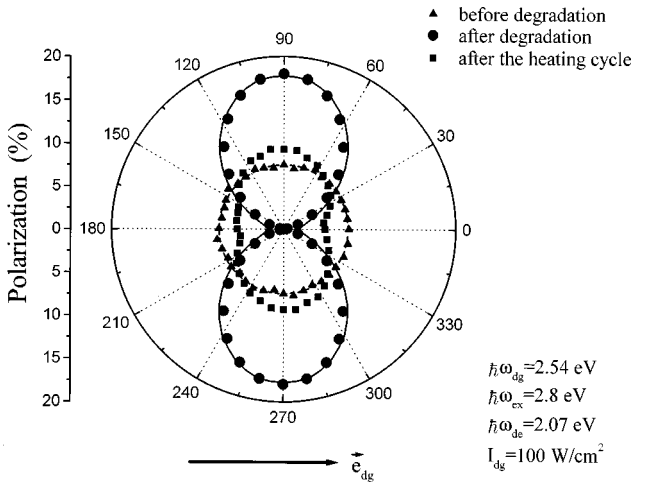

FIG. 6. The effect of low temperature 1.5 K degradation by a twenty minute illumination of a 100 W/cm^2 4880 Å line of a cw Ar^+ degrading laser pump beam on the dependence of the PL polarization on the polarization direction of the probe beam. The direction of the degrading pump beam polarization is indicated by the arrow. Also shown (squares) is the angular dependence of the polarization after a cycle of first heating the sample to 250 K, followed by an immediate rapid cooling back to 1.5 K. The curves are theoretical fits.

$$I_{\mathrm{PL}}\sim\langle N_0(\hat{\mathbf{c}},\mathbf{e}_{\mathrm{ex}})N_0(\hat{\mathbf{c}},\mathbf{e}_{\mathrm{dg}})P(\omega_{\mathrm{ex}})P(\omega_{\mathrm{de}})\rangle, \qquad (15)$$

where $N_0(\hat{\mathbf{c}},\mathbf{e}_{\mathrm{ex}})$ and $N_0(\hat{\mathbf{c}},\mathbf{e}_{\mathrm{dg}})$ are given by Eqs. (8) and (12), respectively. The theoretical curves in Fig. 6 were obtained using Eq. (15) and the same parameters as above and taking $\tau_{AA}=17$ ns, $\tau_T=3$ h, $\tau_r=2.5$ ms, and $\alpha(\omega_{\mathrm{ex}},a)=3.6\times10^{-17}$ cm^2/eV.

As we mentioned above, heating the samples up to room temperature recovers the PL intensity and destroys the optically induced polarization anisotropy. Figure 6 also shows the dynamics of the recovery at intermediate temperatures. The squares in the figure show the degree of polarization after rapidly heating the degraded sample up to 250 K in 15 min and then immediately rapidly cooling it down to 1.5 K in 5 min. One sees that the polarization anisotropy is drastically reduced during this heating cycle. Recovery sets in between 150 and 250 K. For comparison we would like to mention that the polarization anisotropy disappears completely if one holds the temperature at 200 K for 30 min.

VI. DISCUSSION

Our polarization studies of the PL saturation effects and the PL degradation effect allows us to extract some information on the parameters which characterize these nonlinear effects. The analysis is done using the simplifying assumption that all the crystals contributing to the PL at a particular frequency are characterized by an average shape, size, radiative lifetime, and orientation relative to the [100] p-Si growth direction. The weakest part of this assumption is that concerning the radiative lifetimes. Our experimental data clearly show a distribution of radiative lifetimes that vary by as much as an order of magnitude for the crystals emitting

light at the same frequency. This reflects the fact, e.g., that crystals of quite different shapes can emit light at the same frequency but have different radiative lifetimes.[28] The distribution of lifetimes has not been taken into account and makes it difficult to describe the intensity dependence of the PL saturation.

Despite of extreme simplicity of our model, it describes all our experimental data rather well. The best description is obtained for crystals for which the ratio of their minor to major axis varies from 1/4–1/12, and whose major axes are directed 26°–35° from the [100] p-Si growth direction. These parameters correlate well with the data of TEM measurements of similar p-Si samples.[29,30] The values of the average absorption cross section of the nanocrystals, 6.0×10^{-17}, 4.1×10^{-17}, and $2.9\times10^{-17}\,\mathrm{cm}^2$ obtained for the detection energies $\hbar\omega_{\mathrm{de}}=1.55$, 1.77, and 2.07 eV, respectively, are quite reasonable. The decrease of cross section with detection energy is associated with a decrease in crystal size (far from the band edge, the cross section is proportional to the crystal volume).

These cross sections and the absorption coefficient, α_{ab}, measured for our samples: $\alpha_{\mathrm{ab}}=10^3\ \mathrm{cm}^{-1}$ at $\hbar\omega_{\mathrm{ex}}=2.54$ eV, allow us to determine the average crystal concentration: $N=\alpha_{\mathrm{ab}}/\hbar\omega_{\mathrm{ex}}\alpha(\omega_{\mathrm{ex}},a)\approx2.4\times10^{-19}\,\mathrm{cm}^{-3}$. This also gives us an average size $\approx[(1-p)/N]^{1/3}=3.1$ nm for the Si crystallites in our samples which have a porousity of $p=0.7$. These estimates are also consistent with available morphological measurements of similar types of the porous Si samples.[31]

Saturation of the PL at high intensities at room temperature, and the low temperature fatigue effect, affect the PL spectra differently. In the first case the PL is quenched in the low energy part of the spectrum and so the PL line shifts to the blue. This is directly connected with the radiative decay time, which is longer for longer detected light wavelengths, and the pump beam suppresses the low energy part of the spectrum.

The low temperature fatigue effect, however affects mainly the spectra in the 2–2.2 eV range and so the PL line shifts to the red. This is caused by Auger autoionization of nanocrystals, which can occur only if the energy which the electron gains after annihilation of the second e-h pair is enough to overcome the conduction band offset. Both the electron affinity of Si and the position of conduction band edge of SiO_2 with respect to the valence band of Si are about of 4.3 eV. As a result efficient Auger autoionization can take place only in crystallites with an effective energy gap $E_g\geqslant2.15$ eV.

Room temperature PL saturation of the nanocrystals takes place when each nanocrystal is occupied by a single e-h pair: $\tau_r I_{\mathrm{ex}}\alpha(\omega_{\mathrm{ex}},a)\sim1$. In porous Si this happens at very low excitation intensities: $I_{\mathrm{ex}}=2$–$20\ \mathrm{W/cm}^2$ because the radiative decay time in this material is very long, on the order of tens of microseconds.

The persistent fatigue and optically induced polarization anisotropy effects are determined by the very slow return of the electrons back to the crystal: at helium temperature $\tau_T=3$ h. The rate of these processes depends exponentially on the ratio of the depth of the traps that localize the electron in the surrounding nanocrystal matrix to the temperature. This opens an interesting opportunity to observe this effect at room temperature by doping the SiO_2 matrix with impurities that would provide deep traps there.

In conclusion, we have demonstrated strong nonlinear optical effects in the PL of porous Si which have been well described as Auger quenching of the luminescence from nanocrystals which contain unpaired charges or more than one e-h pair. The high efficiency of the nonlinear effects is a result of the large ratio of the radiative decay time (porous Si is an indirect semiconductor) to typical times for Auger processes in nanosize semiconductor crystals. This leads to the saturation of the PL at low excitation intensities that, at room temperature, is coincident with the pump beam, and to persistent PL degradation and optically induced polarization anisotropy at helium temperatures.

ACKNOWLEDGMENTS

D. Kovalev is grateful to the Alexander von Humbolt Foundation for the support. Al. L. Efros wishes to acknowledge the support of the Deuthsche Forschungsgemeinschaft. This work was supported by the U. S. Office of Naval Research.

APPENDIX

Averaging Eq. (6) over the azimuthal distribution of the crystallites in the surface plane of the p-Si film leads to integrals of the form:

$$J_n(I_{\mathrm{dg}})=\frac{1}{2\pi}\int_0^{2\pi}\frac{\cos^n x\,dx}{a_d+2b_d\cos x+\cos^2 x},\tag{A1}$$

where

$$a_d=\frac{1+S_r(2+\kappa_d)}{S_T S_r\kappa_d}\,\frac{\tau_T}{\tau_{AA}+\tau_T}+\left(\frac{2+\kappa_d}{\kappa_d}\right)^2,$$

$$b_d=\frac{2+\kappa_d}{\kappa_d}+\frac{1}{2\kappa_d S_T}\,\frac{\tau_T}{\tau_{AA}+\tau_T}.\tag{A2}$$

Calculation of the integrals that appear in Eq. (13) gives

$$J_0=\sqrt{\frac{\sqrt{(2b_d^2-a_d-1)^2+4b_d^2(a_d-b_d^2)}+1+a_d-2b_d^2}{2(a_d-b_d^2)[(2b_d^2-a_d-1)^2+4b_d^2(a-b_d^2)]}},$$

$$J_1=\sqrt{\frac{\sqrt{(2b_d^2-a_d-1)^2+4b_d^2(a_d-b_d^2)}-1-a_d+2b_d^2}{2[(2b_d^2-a_d-1)^2+4b_d^2(a-b_d^2)]}}-b_dJ_0,\tag{A3}$$

$$J_2=1-2b_dJ_1-a_dJ_0,$$

$$J_3=-2b_dJ_2-a_dJ_1.$$

[1] S. Schmitt-Rink, D. A. B. Miller, and D. C. Chemla, Phys. Rev. B **35**, 8113 (1987).
[2] P. Horan and W. Blau, Phase Transit. **24-26**, 605 (1990).
[3] Y. Z. Hu, S. W. Koch, M. Lindberg, N. Peyghambarian, E. L. Pollock, and F. F. Abraham, Phys. Rev. Lett. **64**, 1805 (1990); Y. Z. Hu, M. Lindberg, and S. W. Koch, Phys. Rev. B **42**, 1713 (1990).
[4] Y. Z. Hu, S. W. Koch, and N. Peyghambarian, J. Lumin. **70**, 185 (1996).
[5] F. de Rougemont, R. Frey, D. Ricard, and C. Flytzanis, Appl. Phys. Lett. **50**, 1619 (1987).
[6] P. Roussignol, M. Kull, D. Ricard, F. de Rougemont, R. Frey, and C. Flytzanis, Appl. Phys. Lett. **51**, 1882 (1987).
[7] M. Ghanassi, M. C. Schanne-Klein, F. Nache, A. I. Ekimov, D. Ricard, and C. Flytzanis, Appl. Phys. Lett. **62**, 78 (1993); C. Flytzanis, D. Ricard, and M. C. Schanne-Klein, J. Lumin. **70**, 212 (1996).
[8] V. A. Kharchenko and M. Rosen, J. Lumin. **70**, 158 (1996).
[9] D. J. Chepic, Al. L. Efros, A. I. Ekimov, V. A. Kharchenko, I. A. Kudriavtsev, and T. V. Yazeva, J. Lumin. **47**, 113 (1990).
[10] L. T. Canham, Appl. Phys. Lett. **57**, 1046 (1990).
[11] L. E. Brus, in *Light Emission in Silicon*, edited by D. J. Lockwood, Semiconductor and Semimetals Vol. 49 (Academic Press, New York, 1996).
[12] P. D. G. Calcott, K. J. Nash, L. T. Canham, M. J. Kane, and D. Brumhead, J. Phys. Condens. Matter **5**, L91 (1993).
[13] M. S. Hybertsen, Phys. Rev. Lett. **72**, 1514 (1994).
[14] A. Kux and M. Ben Chorin, Phys. Rev. B **51**, 17 535 (1995).
[15] J. C. Vial, A. Bsiesy, F. Gaspard, R. Herino, M. Ligeon, F. Muller, R. Romestain, and R. M. MacFarlane, Phys. Rev. B **45**, 14 171 (1992).
[16] D. Kovalev, D. Averboukh, M. Ben-Chorin, F. Koch, Al. L. Efros, and M. Rosen, Phys. Rev. Lett. **77**, 2089 (1996).
[17] M. Koos, I. Pocsik, and E. Vazsonyi, Appl. Phys. Lett. **62**, 1797 (1993).
[18] I. Mihalcescu, J. C. Vial, A. Bsiesy, F. Muller, R. Romestain, E. Martin, C. Delerue, M. Lannoo, and G. Allan, Phys. Rev. B **51**, 17 605 (1995).
[19] C. Delerue, M. Lannoo, G. Allan, E. Martin, I. Mihalcescu, J. C. Vial, R. Romestain, F. Muller, and A. Bsiesy, Phys. Rev. Lett. **75**, 2228 (1995).
[20] A. N. Starukhin, A. A. Lebedev, B. S. Razbirin, and I. M. Kapitonova, [Pis'ma Zh. Tekh. Fiz. **18**, 60 (1992) [Sov. Tech. Phys. Lett. **18**, 535 (1992)].
[21] A. V. Andrianov, D. I. Kovalev, N. N. Zinov'ev, and I. D. Yaroshetskii, Pis'ma Zh. Éksp. Teor. Fiz. **58**, 417 (1993) [JETP Lett. **58**, 427 (1993)].
[22] D. Kovalev, M. Ben-Chorin, J. Diener, F. Koch, Al. L. Efros, M. Rosen, N. A. Gippius, and S. G. Tikhodeev, Appl. Phys. Lett. **67**, 1585 (1995).
[23] H. Koyama and N. Koshida, Phys. Rev. B **52**, 2649 (1995).
[24] P. Lavallard and R. Suris, Solid State Commun. **95**, 267 (1995).
[25] L. D. Landau, E. M. Lifshiz, and L. P. Pitaevskii, *Electrodynamic of Continuous Media*, 2nd ed. (Pergamon, Oxford, 1984).
[26] N. A. Gippius, V. D. Kulakovskii, S. G. Tikhodeev, and A. Forchel, Pis'ma Zh. Éksp. Teor. Fiz. **59**, 527 (1994) [JETP Lett. **59**, 556 (1994)]; P. Ils, Ch. Greus, A. Forchel, V. D. Kulakovckii, N. A. Gippius, and S. G. Tikhodeev, Phys. Rev. B **51**, 4272 (1995).
[27] V. Grivickas, J. Linnros, and J. A. Tellefsen, Thin Solid Films **255**, 208 (1995).
[28] J. B. Khurgin, E. W. Forsythe, G. S. Tompa, and B. A. Khan, Appl. Phys. Lett. **69**, 1241 (1996).
[29] A. G. Gullis and L. T. Canham, Nature (London) **353**, 335 (1991).
[30] M. W. Cole, J. F. Harvey, R. A. Lux, D. W. Eckart, and R. Tsu, Appl. Phys. Lett. **60**, 2800 (1990).
[31] A. Nikolov, V. Petrova-Koch, G. Polisski, and F. Koch, in *Microcrystalline and Nanocrystalline Semiconductors*, edited by L. Brus, M. Hirose, R. W. Collins, F. Koch, and C. C. Tsai, MRS Symposia Proceedings No. 358 (Materials Research Society, Pittsburgh, 1995), p. 423.